Materials Today Bio 25 (2024) 100979

Contents lists available at ScienceDirect

Materials Today Bio

journal homepage: www.journals.elsevier.com/materials-today-bio

Multi-functional composite dressings with sustained release of MSC-SLP and anti-adhesion property for accelerating wound healing

Wu Duan [a,1], Haipeng Wang [b,1], Ziran Wang [b], Zhongjing Ren [b], Xinxin Li [c], Falian He [d], Shaomin Li [e], Yingchun Guan [c], Fuqiang Liu [a,f,g,h], Li Chen [a,f,g,h], Peng Yan [b,*], Xinguo Hou [a,f,g,h,**]

[a] Department of Endocrinology, Qilu Hospital of Shandong University, Jinan, Shandong, 250012, China
[b] Key Laboratory of High-efficiency and Clean Mechanical Manufacture of MOE, School of Mechanical Engineering, Shandong University, Jinan, 250061, China
[c] School of Mechanical Engineering and Automation, Beihang University, Beijing, 100083, China
[d] Nuolai Biomedical Technology Co., Ltd., Taian, China
[e] Institute of Aerospace Special Materials and Processing Technology, Beijing, 100074, China
[f] Institute of Endocrine and Metabolic Diseases of Shandong University, Jinan, Shandong, 250012, China
[g] Key Laboratory of Endocrine and Metabolic Diseases, Shandong Province Medicine and Health, Jinan, Shandong, 250012, China
[h] Jinan Clinical Research Center for Endocrine and Metabolic Disease, Jinan, Shandong, 250012, China

ARTICLE INFO

Keywords:
Multi-functional composite dressing
Anti-adhesion
Unidirectional drainage
MSC-SLP
Exudate management

ABSTRACT

Exudate management is of significant clinical value for the treatment of acute wound. Various wound dressings have been developed to restore the function of injured tissues and promote wound healing, but proper exploiting the healing factors inside exudate and achieving anti-adhesion wound care remains a challenge. Herein, we present a novel multi-functional composite dressing (MCD) by coupling supernatant lyophilized powder of mesenchymal stem cells (MSC-SLP) with a sandwich-structured wound dressing (SWD). The developed MCDs demonstrated unique unidirectional drainage capability, stable anti-adhesion characteristics, and improved wound healing performance. The designed SWD with both superhydrophobic inner surface and liquid-absorption ability of mid layer enables the dressings exhibit desired anti-adhesion property to neoformative granulation tissues, favorable shielding effect to exogenous bacteria, as well as appropriate exudate-retaining capability and unidirectional exudate-absorption property. The introduction of MSC-SLP in SWD was demonstrated to further improve wound healing quality. Compared to medical gauze, the synergic effect of SWD and MSC-SLP significantly accelerates wound healing rate by over 30%, avoids tissue avulsion when changing dressings, and produces a flat-smooth closure surface. More importantly, the wound treated with MCDs presents more skin accessory organs and blood vessels in regenerated tissues than other groups. In vivo/vitro biocompatibility evaluations indicated little toxicity, demonstrating the biosecurity of the developed dressings. The proposed method offers great potential in clinical applications particularly for chronic wound treatments.

1. Introduction

Exudate contains various healing factors, creates a moist environment, and provides support for wound healing [1,2]; while too much or little exudate is unfavorable for wound healing due to the induced wound infections or the insufficiency of nutrients for wound healing especially for chronic wounds [3,4]. How to realize efficient exudate management and make full use of the positive effect of exudate under the premise of avoiding wound infection seems to be imperative in clinical care and receives increasing attention [5,6].

Dressings with good absorption ability, such as traditional gauze, hydrogel and polyurethane (PU) sponges, have been developed to remove the accumulated exudates on wound surface [7–10]. However, exudate absorption is apt to result in an over-wet and adhesive interface between these dressings and wound surface, making the dressings adhere to wound surface through wound scabs or neoformative

* Corresponding author.
** Corresponding author. Department of Endocrinology, Qilu Hospital of Shandong University, Jinan, Shandong, 250012, China
E-mail address: yanpeng@sdu.edu.cn (P. Yan).
[1] Wu Duan and Haipeng Wang have equal contribution.

https://doi.org/10.1016/j.mtbio.2024.100979
Received 1 October 2023; Received in revised form 25 December 2023; Accepted 24 January 2024
Available online 10 February 2024

granulation tissues. As a result, severe wound avulsion occurs when repeatedly replacing dressings, leading to secondary injury on wound and bringing great pain to patients [11–13]. To address this issue, a type of Janus dressing has been reported to quickly remove exudate and create a dry wound environment so that to avoid adhesion between dressing and wound surface [14–20]. For example, Qi et al. developed a nanofiber Janus dressing to drain excessive exudate from wound by taking advantage of the wettability difference between two layers [20]. Of note, the exudate removal also implies the loss of various vital healing factors for wound repair [16,17]. Thereby, how to reach a compromise between exploiting the promoting effect of these healing factors for wound healing and efficiently removing the exudate from wound is a critical issue.

In addition to the proper management of exudate, the introduction of various beneficial factors that inhibit wound infection and favor wound repair is also necessary for an ideal wound dressing [17–21]. In recent studies, silver ions, silica nanoparticles, oxacillin and other anti-bacterial drugs have been proposed to be added into dressings to impart dressings antimicrobial activity [20–24]. As reported by Shen et al., in order to prevent bacterial infection, amoxicillin powders were uniformly encapsulated on the assembled Janus wound dressing to achieve faster wound healing [21]. Zhong et al. developed an asymmetric bacterial cellulose (ABC) wound dressing by incorporating silver-metal organic frameworks (Ag-MOF) and curcumin into ABC membrane, and obtained antioxidant, reactive oxygen species (ROS) scavenging and anti-bacterial activities on dressings [24]. The incorporation of these anti-bacterial drugs into wound dressings can indeed reduce wound infections and favor wound healing, but simultaneously brings more risks of human allergies and drug toxicity in actual applications [20–24]. As a consequence, exploring a novel multi-functional dressing that enables efficient exudate management, avoids tissue adhesion between dressing and wound surface, and accelerates wound repair is not only urgent but challenging.

Hydrogels have been extensively used as carriers in wound dressings since they present favorable biocompatibility and provide extracellular matrix (ECM)-like micro-environments for tissue regeneration [25]. Various biologically active substances or drugs can be loaded into hydrogels and sustainedly released through degradation of hydrogels. Poloxamer hydrogels present desired elasticity and plasticity, allowing it to fit snugly with wound surface to avoid the generation of dead space between wound surface and hydrogels and isolate the wound from external environmental stimuli [26]. Simultaneously, hydrogels enable the wound surface maintain a durable moist environment, providing an advantageous condition for wound healing [27]. For instance, Du et al. prepared a medicated hydrogel through loading the curcumin-phospholipid complex (CPC) into poloxamer hydrogel for wound healing [28]. Compared to curcumin hydrogel, CPC hydrogel showed higher curcumin dissolution and wound healing effect on rat skin wound model especially in early phase.

In this study, we proposed a novel multi-functional composite dressing (MCD) with unidirectional drainage capability and anti-adhesion characteristics, where poloxamer hydrogels loaded with MSC-SLP (H/MSC-SLP) were coated on the inner or mid layer of a sandwich-structured wound dressing (SWD) to promote tissue repair through the paracrine effect of stem cells, as illustrated in Fig. 1. SWD was constructed by assembling inner superhydrophobic (SHO) PDMS layer, mid gauze layer and outer hydrophobic PDMS layer. The stable superhydrophobicity enables the inner layer present excellent anti-adhesion property to both bacteria and cells, protect wound surface from bacterial infections and eliminate tissue avulsion when replacing dressings. Benefiting from the strong absorption ability of mid gauze layer, the excess exudates produced on wound surface can be irreversibly absorbed through the micro-channels designed on inner layer. By coating H/MSC-SLP on SHO PDMS surface or gauze layer, the synergic effect of SWD and the MSC-SLP released from hydrogel was experimentally demonstrated to significantly accelerate wound healing process and eliminate tissue avulsion during wound treatments. Taking advantages of the unique unidirectional drainage and stable anti-adhesion capabilities of SWD, the biodegradable property of hydrogel and the paracrine effect of MSC-SLP, the prepared biocompatible multi-functional composite dressing holds the great promise as an ideal dressing for wound healing.

2. Experimental section

2.1. Materials employed in experiments

The employed PDMS membranes of chemical grade were obtained from Hangzhou Guinie Advanced Materials Co., Itd. (Zhejiang, China). The cotton gauze and medical adhesive tapes were obtained from Lanluo Kangmengda (Shandong, China). 407/188 poloxamer hydrogel, DMEM/F12 (F-12, HyClone, Logan City, UT) and fetal bovine serum (FBS, Gibco, Grand Island, NY) were purchased from Aladdin Reagent (Shanghai) Co., Ltd. *Escherichia coli* and *Staphylococcus aureus* were provided by Novolife International Medical Central (Taian, China). The supernatant lyophilized powders of mesenchymal stem cells (MSC-SLP) were provided by Suzhou Ruilai Biotechnology Co., Ltd.

Depilatory cream (Aifuyi) was provided by Naijing Tongrentang (China). Silicone gaskets with the diameter and thickness of 10 mm and 1.0 mm were provided by Shanghai Liangfei Trading Co., Ltd.

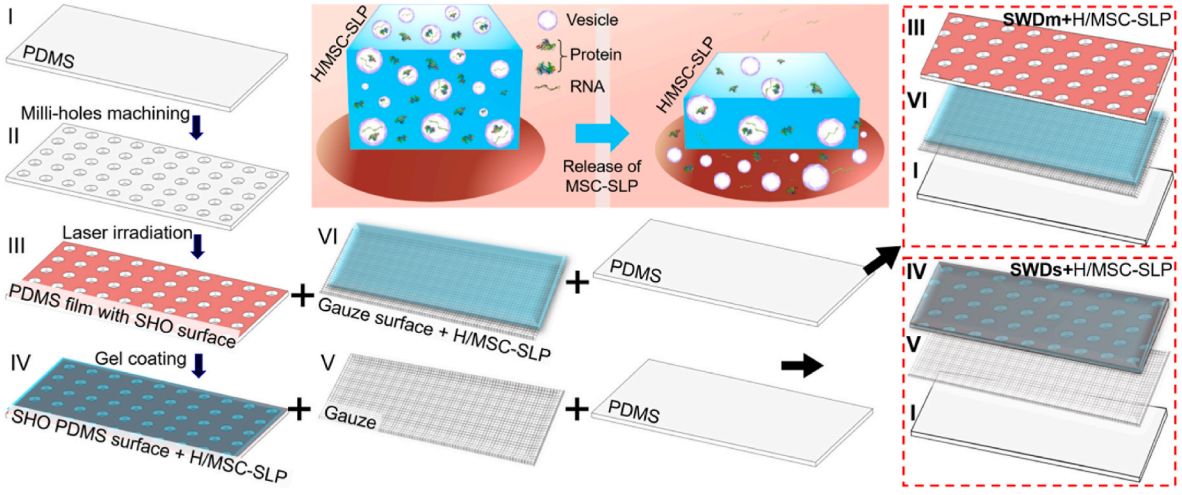

Fig. 1. Schematic diagrams showing the fabrication process of multi-functional composite dressings and the release of the loaded MSC-SLP in hydrogel coating.

(Shanghai, China). Male BALB/c mice 6–8 WEEKS OLD were purchased from Beijing HFK Bioscience Co., Ltd. (Beijing, China) and were maintained in the animal facility of Qilu Hospital of Shandong University. All the mice investigated in our experiments were approved by Animal Procedures Committee of Qilu Hospital of Shandong University. The mice were handled strictly in accordance with the guidelines for the care and use of laboratory animals. All animal care and experimental procedures were reviewed and approved by the Animal Investigation Ethics Committee of Qilu Hospital of Shandong University.

2.2. Preparation of superhydrophobic PDMS surface

Hierarchical micro/nano-structures were fabricated on PDMS surface to obtain superhydrophobicity through femtosecond ultraviolet (UV) laser system (Time Bandwidth; Duetto). The utilized laser parameters mainly include pulse duration of 209 fs, pulse repetition rate of 100 kHz, pulse energy of 4.2 μJ and laser scanning speed of 1000 mm s^{-1}. The geometrical dimensions of the fabricated structures were tuned by controlling the distance between adjacent laser scanning lines and laser scanning repetitions.

2.3. Preparation of various multi-functional dressings

The designed sandwich-structured wound dressing (SWD) is designed to be composed of the outer pristine PDMS layer (thickness 100 μm), the mid gauze layer (thickness 1 mm), and the inner superhydrophobic PDMS layer (thickness 500 μm) with the superhydrophobic surface facing wound surface. The via holes with the optimized diameter of 1.5 mm were machined on PDMS membrane by using a hole punch. Based on previous studies [29,30], hydrogel was obtained by mixing sterile poloxamer 407 (Pol-407, 17.9%) and Pol-188 (8%, w/w) at 4 °C environment. MSC-SLP-loaded hydrogel (H/MSC-SLP) was obtained by dissolving MSC-SLP into hydrogel and maintained at 4 °C environment. By smearing H/MSC-SLP on superhydrophobic PDMS surface or gauze layer of SWD dressing, the dressings of SWDs + H/MSC-SLP or SWDm + H/MSC-SLP was prepared. When preparing dressings, PDMS membranes and gauze were cut of 3 cm × 3 cm, and the dressing was prepared by adhering the three layers together along the edges with medical glue.

2.4. Surface morphology and wettability characterization

The topography and morphology of PDMS membranes were characterized using atomic force microscope (AFM, Bruker BioScope Resolve), scanning electron microscope (SEM, JSM-6610LV) and laser scanning microscope (VK-X100, Keyence). Static contact angle was measured using an DSA100S system (Kruss, Germany) under atmospheric condition. In impinging experiments, dynamic droplet behaviors were recorded with a high-resolution camera equipped in DSA100S system at a frame rate of 1000 fps [31,32]. The experiments were conducted in triplicate for each condition.

2.5. Investigation of unidirectional drainage capability of dressing

The prepared SWD was horizontally fixed, and the 50 μL droplet was deposited using a pipette from both superhydrophobic PDMS and superhydrophilic gauze sides of the dressing. When depositing the droplet onto superhydrophobic PDMS surface, the droplet was gradually squeezed using a pristine PDMS surface until the droplet passed through superhydrophobic PDMS layer. During measurements, the images were captured using a high-revolution camera.

2.6. Bacterial adhesion test

The experiments were divided into two groups, namely pristine PDMS control group and superhydrophobic PDMS (SHO-PDMS) group. *E. coli* and *S. aureus* were dissolved in 1 ml PBS respectively, then the dissolved bacteria were evenly added to the nutrient agar plate (NA), and cultured in a biochemical incubator at 37 °C for 24 h [33]. Disinfected PDMS membranes of appropriate size were placed in bacterial colony of NA for another 24 h. The PDMS were washed three times with PBS and stained with the Annexin V-FITC and the Propidium Iodide (PI) Staining Kit (MultiSciences, Hangzhou, China) according to the manufacturer's instructions. Bacterial density was observed and measured through a electron microscope.

2.7. Cell adhesion test

The experiments were also divided into three groups, namely pristine PDMS control group, SHO-PDMS group and SHO–H-PDMS group. Human Embryonic Kidney HEK-293 T cells (293T) and Human umbilical vein endothelial cells (HUVECs) were cultured in DMEM (Hyclone, Logan, UT) containing 10% fetal bovine serum, 100 IU/mL penicillin, 100 mg/mL streptomycin and incubated at 37 °C in a humidified atmosphere containing 5% CO_2. The SHO PDMS membranes were cut into appropriate sizes, soaked in 75% ethanol for 30 min, washed three times with PBS. Subsequently, the membranes were placed on the bottom of a 6-well cell culture plate with the superhydrophobic facing up. HUVECs and 293T cells were prepared as cell suspensions in DMEM medium. After incubation for 48 h, the supernatant was aspirated, 4% paraformaldehyde was added and incubated for 30 min at room temperature, then the supernatant was aspirated, and washed twice with PBS. Subsequently, the membranes were taken out, placed on a glass slide with the fiber side facing up. The distribution of cells on the film was recorded by a microscope (NIKON ECLIPSE CI, Tokyo, Japan).

2.8. Cell viability and toxicity assay in vitro

Live/dead cell assay: NIH-3T3, HUVEC and HaCaT cells were first seeded on each 6-well culture plate for culture and adhesion for 4 h. For each plate, the six wells were equally divided into three groups. Then the PDMS membranes before and after laser processing were respectively added into two of the six wells and co-cultured with cells for another 48 h, where the used PDMS membranes have the same dimension of 8 mm × 8 mm. Subsequently, the cells in each group were stained by AO-PI kits (Acridine Orange, AO, Propidium Iodide, PI) for live/dead cells assay according to the manufacturer's instructions. Finally, cell viability in each group was assessed using fluorescence microscope (Leica, Germany).

Cell viability and toxicity assays: NIH-3T3, HUVEC, and HaCaT cells were used for cell viability and toxicity assay. For cell viability assay, the three kinds of the cells were respectively cultured in 96-well plates with DMEM containing 10% FBS at 37 °C in a 5% CO_2 atmosphere. In each well, approximately 5000 cells were added. After 4 h of cell adhesion, the wells were equally divided three groups. The PDMS membranes before and after laser treatment were respectively added into one group wells and co-cultured with cells for another 24h, 48h, and 72h, respectively. Then, a volume of 20 μL of CCK-8 solution was added to each well and incubated for another 3 h. The absorbance of each well was measured at the wavelength of 450 nm through microplate reader (Thermo). For toxicity assay, the cells grouping and co-culturing procedures are the same with cell viability assay. LDH kit was used for toxicity assay according to the manufacturer's instructions. The absorbance of each well was measured at the wavelength of 490 nm through above microplate reader. Of note that three independent experiments were repeated in each group for cell viability and toxicity assays.

Cytotoxicity Tests of hydrogel: The hydrogel was dissolved in DMEM medium containing 10% FBS in the proportion of 0%, 1%, 10% and 20%. A volume of 200 μL DMEM medium of cell suspension of NIH-3T3 was dropped into 96-well plates (5000 cells in each well) with hydrogels of different concentrations. The cells and hydrogels were co-incubated for 24 h. A volume of 20 μL of CCK-8 solution was then added to each well and incubated for another 3 h. The absorbance at 450 nm was

measured through a microplate reader (Thermo). Three independent experiments were repeated.

2.9. Cell scratch tests

NIH-3T3, HUVEC, and HaCaT cells were used in experiments. Each type cells were planted in a six-well plate with each well containing 5×10^5 cells. The cells were cultured in high-glucose DMEM medium containing 10% fetal bovine serum (FBS) at 37 °C in a 5% CO_2 atmosphere. When the cell fusion rate reached 80–90%, we used a 200 μl pipet tip to slide vertically along the bottom of the cell culture plate. Afterwards, the supernatant were removed and the floated cells were washed with PBS. And 2 ml of FBS free high glucose DMEM medium was added to each well for continued observation. For each type cells, in addition to the control well (addition of nothing), experimental groups with addition of low concentration exosome (2×10^9 particles/well), high concentration exosome (1×10^{10} particles/well), low concentration MSC-SLP (1 μg/well), and high concentration MSC-SLP (5 μg/well) groups were also set. After 18–24 h, the proliferation and migration states of the cells were observed under optical microscope.

2.10. Release characteristics of the MSC-SLP loaded in hydrogel

20 mg MSC-SLPs were first mixed with the prepared 10 ml hydrogel solution. Then the mixed hydrogel solution was transferred to a 50 ml centrifuge tube and placed in a refrigerator at 4 °C for 6 h to remove the bubbles and fully liquefy the hydrogel. After that, the hydrogel solution was incubated at 37 °C for 6 h to allow it to fully gelify. Then 10 ml preheated DMEM culture medium was added on top of hydrogel (sample). Such sample was repeated in six 50 ml centrifuge tubes. Then the upper layer culture medium was drawn in one tube every 2 h in sequence. After 12 h, the protein concentrations in the solutions were measured using bicinchoninic acid (BCA) method according to the instructions.

2.11. In vivo imaging characterizations

2 mg MSC-SLP was dissolved in 1 ml hydrogel solution. 100 μl of 5 mM CY7 dye (Catalog no. HY-D0825, MCE, USA) was added in above solution and mixed well in dark for 15 min. Then the hydrogels loaded with MSC-SLP were used to prepare SWDs + H/MSC-SLP or SWDm + H/MSC-SLP dressings. The dye-containing dressings were applied on the created diabetic wounds on mice, and the fluorescence signals around wound were collected at 0 h, 12 h, and 24 h using an In Vivo Imaging System (Tanon company, Shanghai, China). After 24 h, the mice were euthanized, and blood, urine and various internal organs were collected for fluorescence signal detection.

2.12. Induction of diabetes

6–8 weeks old male BALB/c mice were rendered diabetic by high fat feeding for 4 weeks and intraperitoneal injection of 200 mg/kg streptozotocin (STZ; Sigma-Aldrich, St Louis, MO, USA). Blood sugar was monitored using a glucose meter (Roche Diagnostics, Mannheim, Germany). Animals with two consecutive daily blood glucose measurements above 20 mmol/l were considered diabetic and were performed skin wound surgery.

2.13. Study on the treatment effect for diabetic wound healing model

Diabetic BALB/c with a model of back skin wounds were divided into 6 groups mice treated with (1) ordinary medical gauze, (2) SWD, (3) H/MSC-SLP + G, (4) SWDm + H/MSC-SLP, (5) SWDs + H/MSC-SLP and (6) SWDm/s + H/MSC-SLP. There were 3 mice in each group. The mice were anesthetized with pentobarbital sodium. The hair in the center of mice back was depilated through epilator and depilatory ointment. A skin biopsy device was used to punch a hole with the diameter of 8 mm. The round skin wound presents a sharp cut edge. Cotton swabs was used to press wound to stop bleeding, and silicone rings were used to fix the wound to avoid the impact of mechanical traction on wound healing. According to different groups, the wound was first covered with a dressing, followed by a medical adhesive bandage. The dressings were changed every 3 days. The wound size was recorded using a vernier caliper, and the evolution of wound appearance was recorded using a camera. ImageJ software was used to calculate wound area for statistics analysis of the wound healing rate. At the end of the experiment(at day 15), the mice were anesthetized and euthanized, and the newborn skin tissue of the back was removed for further observation.

2.14. Histopathological analysis

The collected skin tissue was fixed with 4% paraformaldehyde for 24 h, then dehydrated with 15% and 30% sucrose solutions for 24 h and 12 h, respectively. Later, dehydrated skin tissue was placed in an embedding box and embedded with optimal cutting temperature compound. The tissue was sectioned to the thickness of 6 μm, and then conventional H&E, CD31 and masson staining was performed. After sealing the tissue, the tissue was observed and photographed under ordinary microscope and fluorescence microscope.

3. Results and discussion

3.1. Material characterizations

Polydimethylsiloxane (PDMS) membranes and gauze were applied to construct SWD with the aid of laser micro/nano-manufacturing process (Fig. 1), where the milli-holes were machined through mechanical drilling and the superhydrophobic surface was fabricated through laser irradiating on PDMS surface. Surface morphology of pristine PDMS membrane was measured through SEM and AFM. As observed in Fig. 2a and b, where the inset image in Fig. 2a showed the morphology on pristine PDMS surface with higher magnification, the pristine PDMS membrane was constructed of numerous closely interconnected nanopores with the dimension ranging from tens to hundreds of nanometers. The intrinsic chemical compositions and porous surface morphology endowed PDMS membrane with good surface hydrophobicity, where the droplets of water, FBS and F12 on pristine PDMS surface presented a contact angle of 106.2°, 93.0° and 95.0°, respectively (Fig. 2e). These droplets strongly adhered on the surface and do not slide off even when the surface tilted at 90°.

Constructing hierarchical micro/nanostructures with specific characteristics on hydrophobic surface is a common strategy to realize superhydrophobic property [34,35]. Fig. 2c shows the laser fabricated hierarchical micro/nano-structures consisting of the microcones array (Fig. 2c) and the densely distributed nanoparticles on microcones surfaces (inset image in Fig. 2c), where the microcones have an average height of 60 μm and an adjacent distance between microcones of 120 μm. Fig. 2d shows the three-dimensional morphology of laser fabricated microcones on PDMS surface, which indicates that the formed microcones present regular shapes and uniform dimensions in height and diameter. Thus, the resultant structured surface in large area presents uniform properties, e.g. surface wettability. As observed in Fig. 2e and f, these structured surfaces exhibit superhydrophobic property and present low adhesion to various liquids, where water, FBS and F12 on the structured surfaces present a contact angle of over 150° and a sliding angle of less than 10° (Fig. 2e). Fig. 2f shows the dynamic behaviors of various droplets impinging on the structured surface, which is used to evaluate the stability of superhydrophobicity. The falling water droplet first underwent a lateral spreading process (0–3 ms) when contacting superhydrophobic surface, then retracted and rebounded up (3–7 ms), and completely separated from the surface (7–15 ms), followed by several fall-rebound cycles, and finally rolled off the surface. In contrast,

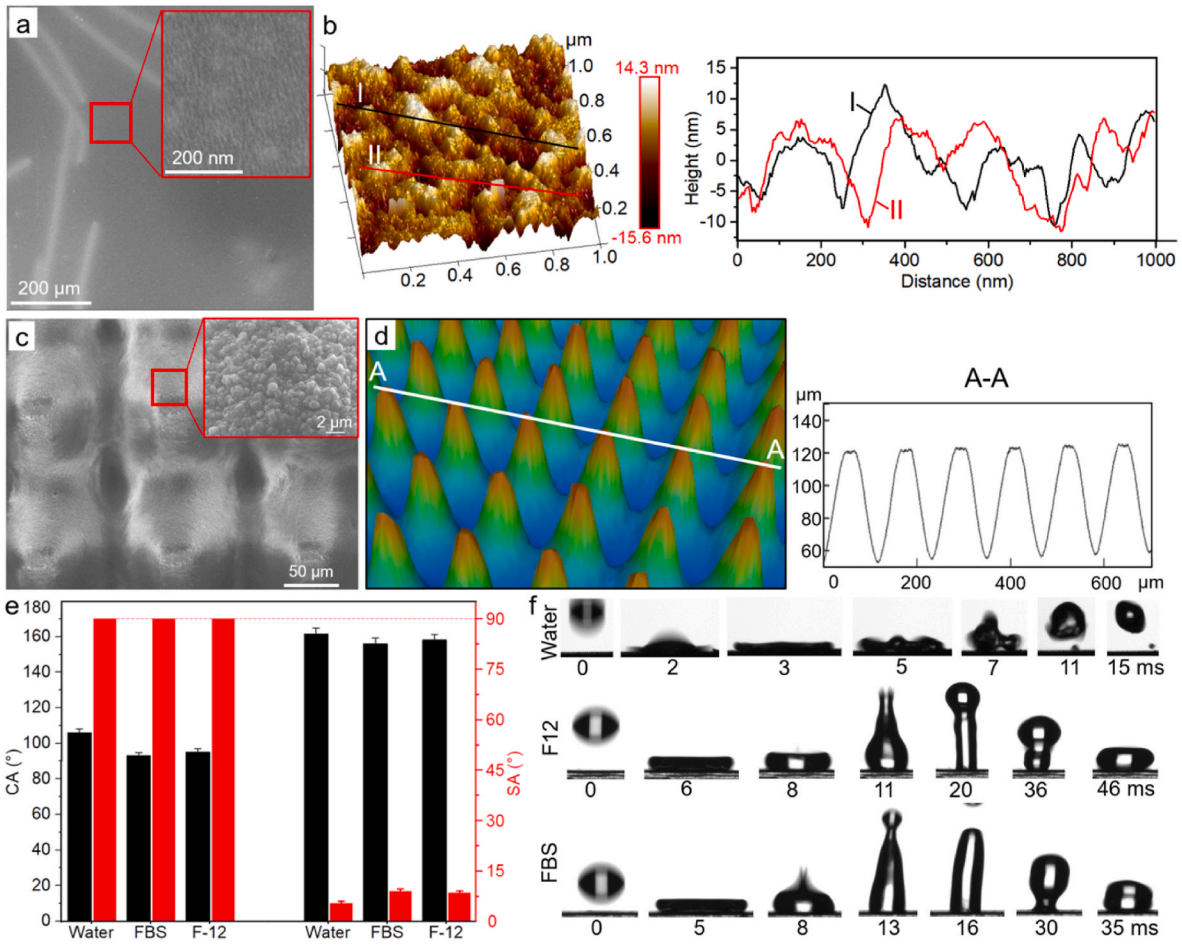

Fig. 2. Morphology and wettability characteristics of PDMS surfaces before and after laser processing. a-b) Surface morphologies and typical height profiles of nanopores on pristine PDMS membrane. c-d) Surface morphologies and typical cross-sectional profiles of the laser fabricated hierarchical micro/nano-structures on PDMS membrane, where the height of microcones is approximately 60 μm and the interspace distance between microcones is 120 μm. e) Contact angle and sliding angle of various droplets on PDMS surfaces with different morphology. f) Dynamic processes of various droplets impinging on the structured PDMS surface.

the falling FBS or F12 droplets finally adhered on the surface after impact, without detaching from surface in retracting process (Fig. 2f). Both the droplets stabilized on surface with an ellipsoid shape. The Cassie-to-Wenzel translation at solid-liquid interface is responsible to the high adhesion of the interface to droplets, but droplets on the structured surface retain a superhydrophobic state. The results demonstrated strong stability of the superhydrophobicity, which laid the foundation for subsequent preparation of MCDs and SWDs.

3.2. Anti-adhesion properties of superhydrophobic PDMS surface

Wound healing is generally a complex process, especially for chronic wounds such as diabetic wound, due to bacterial infection. Imparting anti-bacterial adhesion property to dressing is an important strategy to reduce wound infections [36,37]. Compared with conventional anti-bacterial materials containing Ag ions or antibiotics, superhydrophobic surface shows low cytotoxicity and remains good anti-adhesion properties [38,39]. Anti-adhesion performance of superhydrophobic PDMS surface to bacteria was evaluated by culturing *E. coli* and *S. aureus* on PDMS membranes. When lifting the membranes from nutrient agar plate, large amount of bacteria (both *E. coli* and *S. aureus*) were strongly adhered on pristine PDMS surface (Fig. S1), where the area ratio of *E. coli* and *S. aureus* on pristine PDMS surface reached up to 61.6% and 68.2%, respectively. By contrast, few bacteria were adhered on SHO PDMS surface, where the area ratio of *E. coli* and *S. aureus* on SHO PDMS surface was 11.9% and 3.2%, respectively. After washing and staining process, as displayed in Fig. 3, numerous *E. coli* colonies (area ratio of 16.2%) and densely distributed *S. aureus* (1.05×10^6 mm^{-2}) adhered on pristine PDMS surface, indicating high adhesion of the surface to both bacteria. In contrast, nearly no bacteria were observed on superhydrophobic PDMS surface, indicating low adhesion of the structured PDMS surface to *E. coli* and *S. Aureus*. The anti-adhesion performance of superhydrophobic PDMS surface was also performed by culturing 293T and HUVEC cells on PDMS membranes. As observed in Fig. 3b, the densely distributed 293T cell groups (25 groups/mm^2) and HUVEC cells (587 cells/mm^2) were observed on pristine PDMS surface, while few cells were detected on superhydrophobic PDMS surfaces. The low cell adhesion performance of superhydrophobic PDMS surface was mainly ascribed to the low contact area of the cells to surface and the unfavorable growth environment on superhydrophobic PDMS surface [40,41]. When used for preparing dressings, the excellent anti-adhesion performance of superhydrophobic PDMS surface provides great promise for reducing the tearing of wound tissues and secondary wound injury [42,43].

3.3. Preparation of multi-functional composite dressing

The sandwich-structured wound dressing (SWD) is prepared by assembling a SHO PDMS membrane with milli-scale via holes as inner layer, a gauze layer to absorb excess exudate on wound surface, and a pristine PDMS membrane as outer layer to protect wound from infections by external pathogens (Fig. 1), where the milli-holes function as

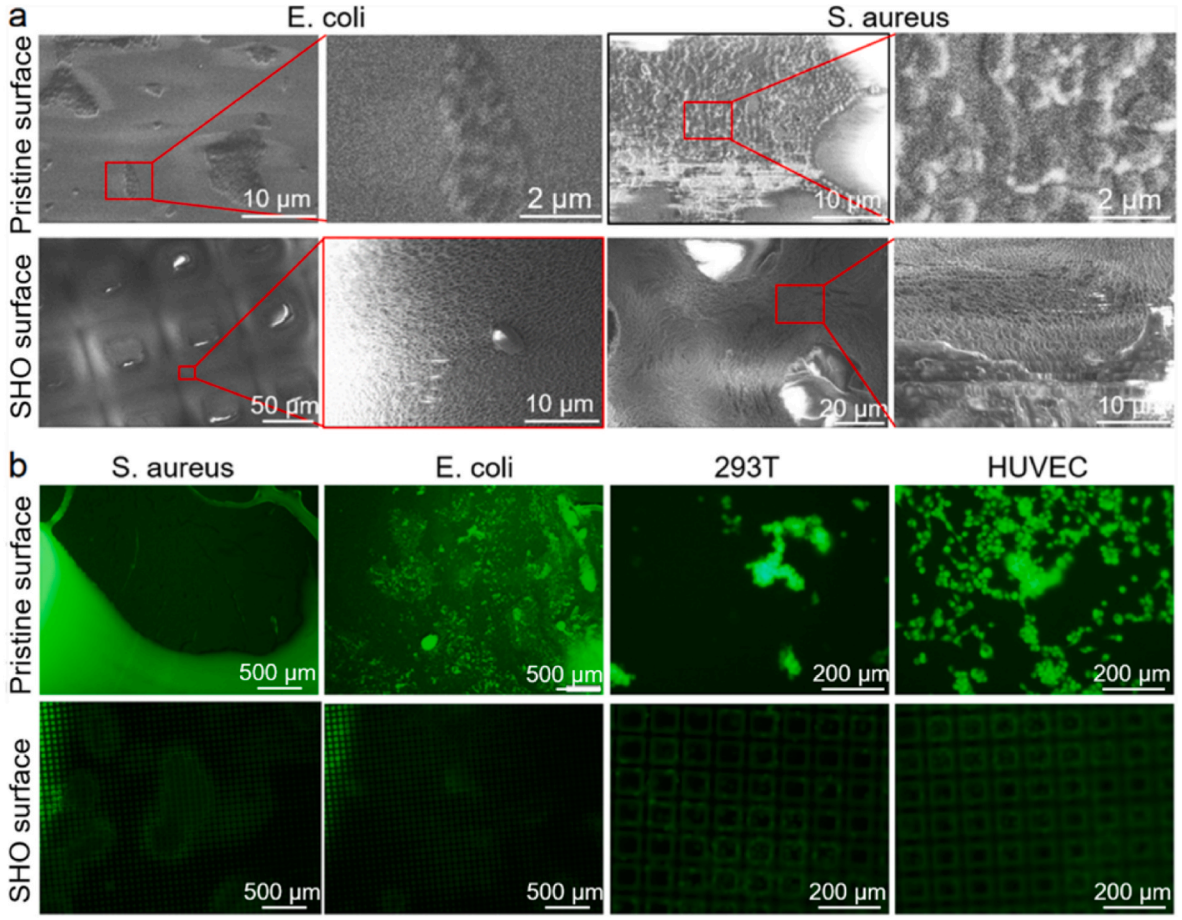

Fig. 3. The anti-adhesion properties of PDMS surface with different hierarchical structures. a) SEM images showing the anti-bacterial property of pristine and superhydrophobic PDMS surfaces to *E. coli* and *S. aureus*. b) Fluorescence microscope images showing the anti-bacterial and anti-cell adhesion properties of pristine and superhydrophobic PDMS surfaces.

channels to realize unidirectional drainage capability at the interface between SHO PDMS and gauze layers. The unidirectional drainage effect of SWD was physically simulated as schematically illustrated in Fig. S2 (a), where the droplet represents the accumulated exudate on wound surface. When droplet was dropped on SHO PDMS surface, the droplet could be drained into milli-holes and absorbed by gauze layer under the squeezing effect from a PDMS surface, where the squeezing effect represents the interaction between dressing and wound surface. On the contrary, when droplet was dropped from gauze side, the liquid was quickly absorbed by gauze layer, but liquid diffusion ended at the interface between gauze and PDMS layers (Fig. S2(b)). The above results demonstrate the potential unidirectional drainage capability of the designed sandwich-structured dressings. Thus, these dressings exhibit potential abilities of protecting wound from external fluids, removing excess exudate from wound and maintaining anti-adhesion performance of the dressings.

When introducing MSC-SLP in SWD, the wound healing process is expected to be further accelerated due to the promoting effect of MSC-SLP in cell proliferation. In our experiments, MSC-SLPs were evenly dissolved into poloxamer hydrogel to prepare the mixed gel (H/MSC-SLP). By loading H/MSC-SLP on SHO PDMS surface or mid gauze layer, two different multi-functional composite dressings of SWDs + H/MSC-SLP and SWDm + H/MSC-SLP were prepared, as illustrated in Figs. 1 and 4. When applied SWDs + H/MSC-SLP on wound surface, the H/MSC-SLP layer was tightly contacted with wound surface (Fig. 4, left). The large contact area between H/MSC-SLP and the exudate on wound surface enabled hydrogel to degrade quickly, leading to the release of numerous MSC-SLPs into wound surface to facilitate wound repair. However, the close contact of the H/MSC-SLP layer with wound surface simultaneously led to severe adhesion at the interface, which brought great challenge for dressing replacement. In comparison, when applied SWDm + H/MSC-SLP on wound surface, much less hydrogels were

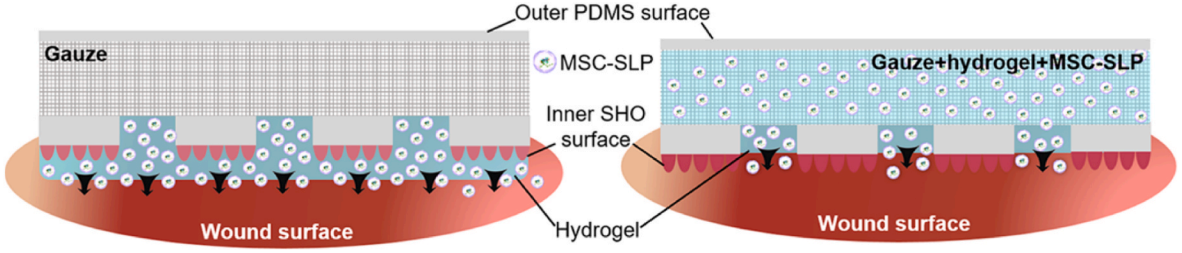

Fig. 4. The release of the MSC-SLPs loaded in hydrogel coated on inner SHO PDMS surface (left) or mid gauze layer (right).

exposed to wound surface and the released small amount of MSC-SLPs from hydrogel contributed to wound healing; meanwhile, the inner SHO PDMS surface enabled the dressing difficult to be adhered to wound surface, which provided great convenience for dressing replacement during wound healing.

The diabetic wound is commonly known to be difficult to heal, which is mainly attributed to the vascular reconstruction disorder, local inflammation, glucotoxicity, and matrix production disorders. The supernatant of stem cells contains abundant various cytokines (VEGF, EGF, FGF, TGF-β), exosomes and anti-inflammatory factors, which promote vascular regeneration, fibroblast differentiation, deposition of extracellular matrix such as collagen, as well as anti-inflammation and fibroblast migration to facilitate wound healing [44–46]. These bioactive substances are well preserved in the MSC-SLPs used in our experiments. The most important cytokines for promoting wound healing, including the vascular endothelial growth factor (VEGF), the epidermal growth factor (EGF) and the exosomes in MSC-SLPs, have been detected using enzyme linked immunosorbent assay (ELISA) and nanoparticle tracking analysis (NTA) methods when the lyophilized powders are completely restored to original supernatant concentration (e.g., Fig. S3), where the concentrations of VEGF, EGF and exosome is 7.36 pg/ml, 16.24 pg/ml and 5.7 $\times$ 10^9 particles/mL, respectively. In actual applications, the concentration of these bioactive substances dissolved in wound exudate is much higher than that in supernatant. Particularly, the biological functions of extracellular vesicles (exosomes) from stem cells in diabetic wounds healing, such as anti-inflammatory [47,48], promoting angiogenesis [49,50] and facilitating cell proliferation and migration [51,52], have been widely reported in previous investigations.

To evaluate the biological effects of MSC-SLP, cell scratch tests have been carried out using the representative fibroblasts (NIH-3T3), endothelial cells (HUVEC), and epidermal keratinocytes (HaCaT) that make up the skin. Compared with control group, the addition of exosome contributed to the proliferation and migration of NIH-3T3 and HUVEC cells to a certain extent, while the addition of MSC-SLP significantly accelerated the proliferation and migration of NIH-3T3 and HUVEC cells, as clearly observed in Figs. S4(a–b). In contrast, the addition of both exosome and SLP contributed little to the proliferation and migration of HaCaT cells (Fig. S4(c)). Therefore, compared with exosome, the introduction of MSC-SLP in the prepared dressings shows higher potential to promote wound healing. Moreover, the diabetic wound healing process includes inflammatory, proliferative, and remodeling phases. The various bioactive substances in MSC-SLP function their biological effects over the whole healing process [47]. For instance, the exosomes and anti-inflammatory factors function their effects in early inflammatory phase, while various reparative cytokines function their effects in subsequent proliferative and remodeling phases [50,52,53].

The release characteristics of the loaded MSC-SLP in hydrogel was tested in DMEM culture medium. As displayed in Fig. S5, the loaded MSC-SLPs in hydrogel were gradually released with time due to the degradation of hydrogels in DMEM culture medium. Simultaneously, the MSC-SLP concentration in the medium increased with time at nearly a liner trend. To validate that the loaded MSC-SLP in hydrogel can be effectively released and absorbed by wound exudate during applications, the wounds treated by SWDs + H/MSC-SLP and SWDm + H/MSC-SLP dressings were respectively characterized using CY7 dye. As indicated in Figs. S6(a–b), the loaded MSC-SLPs in both SWDs + H/MSC-SLP and SWDm + H/MSC-SLP dressings have been detected within and around the wounds of two models, especially when both the wounds were treated for more than 12 h. Furthermore, after the wounds were treated for 24 h, the mouse organs were harvested for fluorescence detection. As observed in Figs. S6(c–d), the fluorescence signals have been detected in the liver, spleen, kidney and blood from both mice, indicating that the bioactive substances in MSC-SLPs have entered the bloodstream, liver, spleen and kidneys. All these experimental results demonstrate that the loaded MSC-SLPs in both SWDs + H/MSC-SLP and SWDm + H/MSC-SLP dressings can be continuously released and successfully absorbed by wound exudate to function their biological effects during wound healing.

3.4. *In vivo excisional wound healing study*

Based on the presented capabilities of SWD and the promoting effect of MSC-SLP in cell proliferation, *in vivo* experiments were conducted to evaluate the effect of the prepared various dressings on wound healing process. Diabetic acute wound model was created on the center of mice back as shown in Fig. 5a, then the wounds were treated with different dressings, namely control (gauze), SWD (sandwich-structured wound dressing), H/MSC-SLP + G (gauze loaded with H/MSC-SLP), SWDm + H/MSC-SLP (SWD loaded with H/MSC-SLP on mid gauze layer), SWDs + H/MSC-SLP (SWD loaded with H/MSC-SLP on SHO PDMS surface), and SWDm/s + H/MSC-SLP (SWDm + H/MSC-SLP in first 3 days while SWDs + H/MSC-SLP in later period) groups. The wound healing process was tracked over a 15-day period, where the dressings were replaced and the repaired wound surfaces were recorded every 3 days. In early period (within 3 days), the wound is in the acute inflammatory phase, a large amount of exudates are produced on wound surface. As observed in Fig. S7, severe tissue adhesion generated between wound surface and gauze or H/MSC-SLP in control, H/MSC-SLP + G and SWDs + H/MSC-SLP groups, leading to avulsion of neoformative granulation tissues on wound surface when replacing dressings (Video S1, Video S3, Video S5). In comparison, little adhesion was observed at the interfaces between dressing and wound surface in other groups (SWD, SWDm + H/MSC-SLP) (Video S2, Video S4), which benefited from the stable superhydrophobic and anti-adhesion properties on PDMS surface and the unidirectional drainage capability of SWD.

The images in Fig. 5b documented the development of wound healing under the different treatments at 0, 3, 6, 9, 12 and 15 days. As a whole, the wound size in all six groups reduced over time, as observed in Fig. S8. The wounds in Control, SWD and SWDs + H/MSC-SLP groups showed small closure and low healing rate (Fig. 5b and c), even the wound size was enlarged (Control group) at day 3. In comparison, the wounds in SWDm + H/MSC-SLP and SWDm/s + H/MSC-SLP groups showed larger closure and exhibited higher healing rate throughout the whole period, which mainly benefiting from the positive effect of exudate and H/MSC-SLP on tissue repair and the timely removal of excess exudate through unidirectional drainage effect of SWD. However, the wound healing in SWDm + H/MSC-SLP group gradually became slower than that in SWDm/s + H/MSC-SLP group in later period, due to different availability of bioactive substances such as exosomes from dressings for wound healing. In later period, wound healing progressed to proliferation stage and exudates produced on wound surface became less, the adhesion generated between dressing and wound surface reduced significantly [54]. Meanwhile, the MSC-SLPs loaded in SWDm/s + H/MSC-SLP group were sustainedly released through the degradation of hydrogel during the direct interactions between wound exudate and the H/MSC-SLP on dressing surface. By comparison, most of the MSC-SLPs loaded in SWDm + H/MSC-SLP group were isolated by the inner SHO PDMS layer of dressing and much less MSC-SLPs were released to exert functions for wound healing, leading to lower healing rate. Notably, the wound treated in H/MSC-SLP + G group still exhibited high healing rate, though severe avulsion of neoformative granulation tissues repeatedly occurred when replacing dressings. This is mainly ascribed to the strong promoting effect of the released MSC-SLP from hydrogel on wound healing and the excellent breathability of gauze.

Overall, the wound treated in SWDm/s + H/MSC-SLP group exhibited superior healing quality during the whole period, owing to the synergetic effect of the anti-adhesion property of SWDm + H/MSC-SLP to wound surface in early period, the excellent unidirectional drainage capability and moisturizing performance of dressing, and the strong promoting effect of MSC-SLP on wound repair in later period. In this

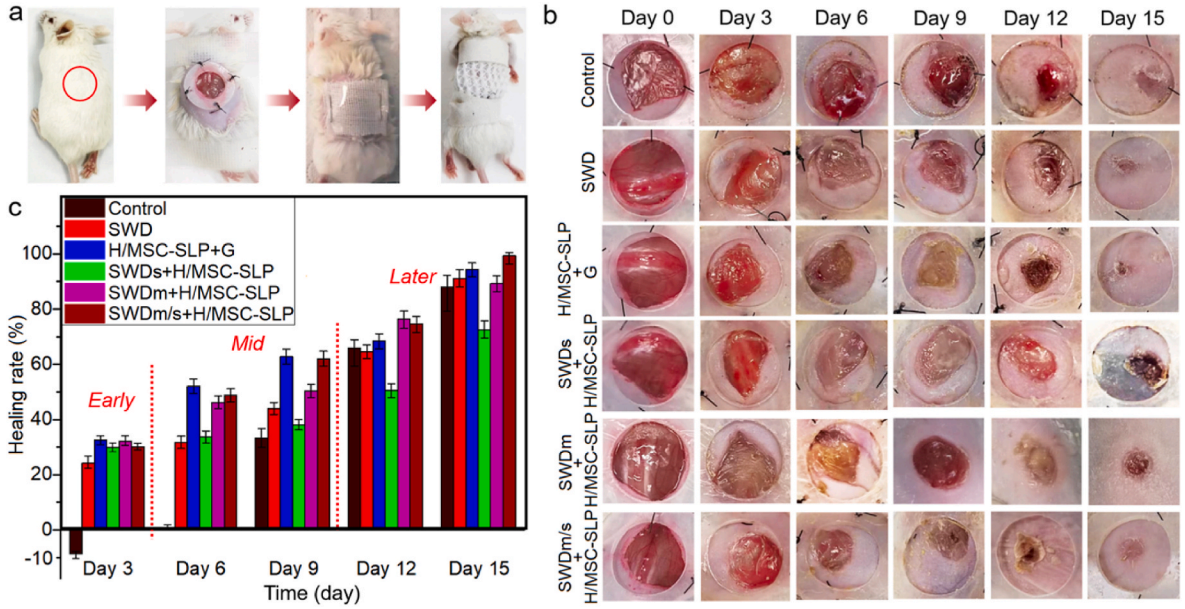

Fig. 5. a) Diabetic acute wound model constructed on mice back. b) Evolution of the wounds treated with gauze (control), SWD, H/MSC-SLP + G, SWDm + H/MSC-SLP, SWDs + H/MSC-SLP, and SWDm/s + H/MSC-SLP, respectively. c) Statistical analysis of the healing rate of the wounds treated with different dressings.

group, severe avulsion of neoformative granulation tissues was effectively avoided in early wound healing period when large amount of exudate generated on wound surface, which was conducive to wound healing; moreover, the released MSC-SLP from H/MSC-SLP fully exerted its promoting effect on wound repair in later wound healing period. Compared with control group, the wound healing rate was accelerated by over 30% at the same phase, as observed in Fig. 5c.

3.5. Histological assessment

To further evaluate the wound healing quality, the full-thickness skin layers of the wounds treated with different dressings were completely

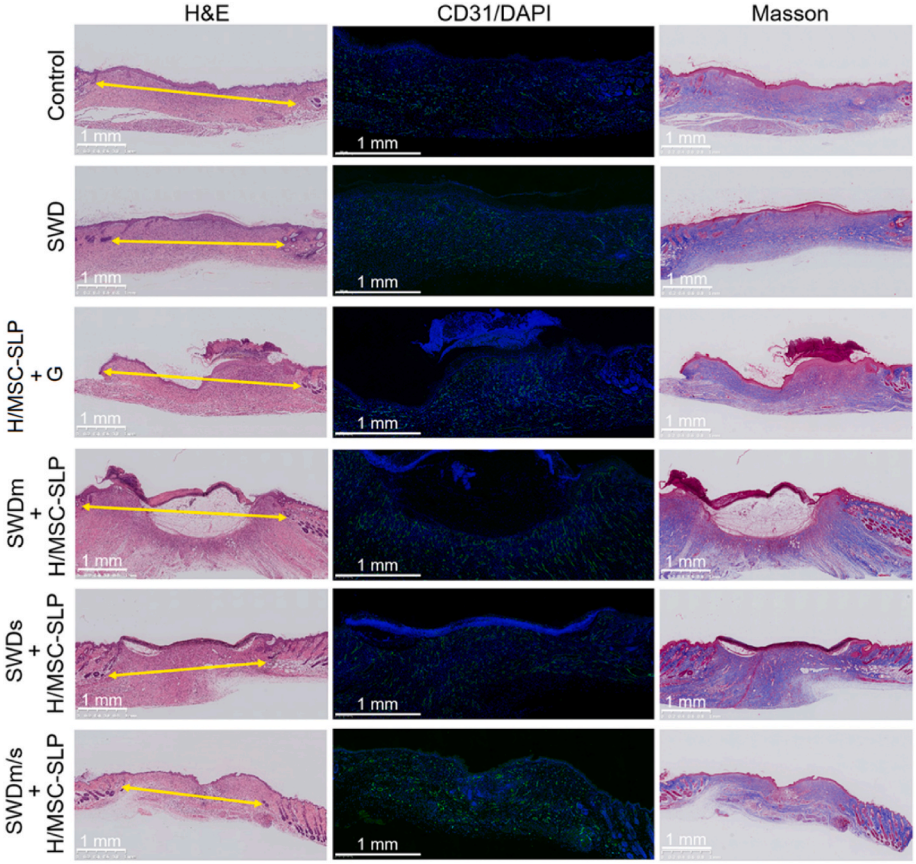

Fig. 6. H&E, CD31 and Masson's staining of the skin tissue around wounds.

removed at day 15 for histological analysis using HE staining, CD31 immunofluorescence staining and Masson staining (Fig. 6). It can be seen from Fig. 5 that the wound edge of epidermis layer in control group is irregular, which is presumed to be caused by the tissue avulsion when changing dressings. Since the gauze possesses lattice-like porous structures with hole size of approximately 0.8 ± 0.1 mm and provides favorable condition for neoformative granulation tissues to grow into the holes, leading to severe adhesion between gauze and tissues. Thus, the tissue avulsion occurred when replacing dressings results in rough wound edges. In SWD group, the repaired wound surface shows regular shape (Fig. 6). Meanwhile, small amount of skin appendages and a thin subcutaneous collagen layer were obtained. In both H/MSC-SLP + G and SWDs + H/MSC-SLP groups, obvious traces of tissue pulling were observed due to the strong adhesion of neoformative granulation tissues to hydrogel. On the one hand, the adhesion derives from the physical sticky property of hydrogels to wound surface [29]. On the other hand, the porous structures of hydrogels also provide the possibility for the cells to grow into hydrogels.

The pulling of tissue is conducive to alignment healing of wound to some extent, but is more likely to result in the generation of folds and scarring in the repaired wound surface (Fig. 5b and Fig. S7). In SWDm + MSC-SLP group, the unidirectional drainage capability and anti-adhesion property of SWD as well as the loaded H/MSC-SLP in gauze layer played indispensable roles in removing exudate from wound surface, avoiding adhesion between dressing and wound surface, and promoting wound healing in early period, but lost its advantages in later stages (after day 6, Fig. 5c). The wound in this group presents a higher depth, generates much more necrosis exudes and shows lower healing speed than that in other groups in the healing process, leading to a crater-like shape on the repaired wound surface (Fig. 6).

In SWDm/s + H/MSC-SLP group, a large amount of exudates generate on wound surface in early wound healing period, the sandwich-structured dressing with H/MSC-SLP loaded in mid layer (SWDm + H/MSC-SLP) can effectively remove excess exudates from wound surface through unidirectional drainage effect of SWD [31], which protects the wound healing process from being influenced by the excess exudates induced hypoxia and avoids the generation of pathogens. After 6 days, the wound healing process passed through acute exudative period and a cellulosic cap formed on wound surface. The cellulosic cap is packed with tissue matrix such as mucin and fibrin, and serves as a barrier to the stimulation from external environment to some extend. In this period, loading H/MSC-SLP on SWD surface (SWDs + H/MSC-SLP) is beneficial to directly exert the biological effect of MSC-SLP in promoting wound healing through the degradation of hydrogel [55]. Simultaneously, the results in immunofluorescence staining of the characteristic marker CD31 of vascular endothelial cells suggests that more neovascularization were observed in SWDm/s + H/MSC-SLP group than that in other groups (Fig. 6). As a consequence, the wound in SWDm/s + H/MSC-SLP group shows the highest healing speed and presents the best healing quality.

3.6. Evaluation of in vitro cytotoxicity and in vivo biocompatibility

The cytotoxicity of PDMS membranes before and after laser treatment was first evaluated by co-culturing PDMS membranes with NIH-3T3, HUVEC, or HaCaT cells in cell suspension for 24 h, 48 h, and 72 h, respectively. As displayed by the CCK-8 and LDH assay results shown in Figs. S9(a–f), compared with control group (pure suspension), cell viability of NIH-3T3, HUVEC, and HaCaT cells in the suspension co-incubating with pristine or SHO PDMS membrane changes little. The cells in all the groups show similar proliferation rate when incubation time increased from 24 h to 72 h (Figs. S9(a–c)), and the cell cytotoxicity in all the groups shows no obvious increase with time (Figs. S9(d–f)). Furthermore, the live/dead cell assays were also performed by incubating NIH-3T3, HUVEC, or HaCaT cells with PDMS membranes for 48h. Then the cell viability was characterized through fluorescence microscope, where the live cells were stained by AO (green) and the dead cells were stained by PI (red). As shown in Fig. S10, there are nearly no dead cells were observed in all the groups in the images. These results indicated that the PDMS membranes before and after laser irradiating had no potential cytotoxicity.

The influence of 407/188 poloxamer hydrogels on the viability of NIH-3T3 cells was also evaluated using CCK-8 assay. Poloxamer hydrogel solutions with different volume concentrations were added into the culture system of NIH-3T3 cells. After 24 h, the viability of NIH-3T3 cells in different hydrogel solutions was detected. As shown in Fig. S11, when hydrogel concentration increases to 10% and above, cell proliferation is obviously suppressed. Thus, the direct utilization of hydrogel on wound surface is not considered an positive method to promote wound healing. In our experiments, the hydrogels mixed with MSC-SLP were loaded onto the surface of dressing to exert the functions of MSC-SLP through the degradation of hydrogels in exudate.

After being treated with different dressings, the mice were killed at day 15 and the main organs (heart, liver, spleen, lung and kidney) of mice were stained with H&E for pathological analysis. As shown in Fig. 7, no significant organ damage, histological abnormity or inflammatory lesions was observed in the H&E staining photos of heart, liver, spleen, lung, and kidney among all the treated groups, suggesting that all the as-prepared dressings were nontoxic and bio-safe. Further, we performed serum biochemical analysis on day 15 through canthus vein blood collection. As observed in Fig. 8, no significant difference in blood biochemical indicators, including total protein (TP), albumin (ALB), globulin (GLB), alkaline phosphatase (ALP), alanine transaminase (ALT), aspartate transaminase (AST), AST/ALT, total bilirubin (TBIL), indirect bilirubin (IBIL), UREA, and uric acid (UA) was found among all the groups. Thus, the application of PDMS and poloxamer hydrogels loaded with MSC-SLP has little side effect on the blood biochemical indicators, suggesting good biocompatibility of the as-prepared various dressings and little side influence of the dressings on the functions and metabolism of liver and kidneys.

4. Conclusion

In summary, we have demonstrated a novel multifunctional composite dressing with unidirectional drainage capability and anti-adhesion property to improve cutaneous wound healing efficiency. The stable superhydrophobicity on inner PDMS layer enables the dressings present strong exudate-repellency and anti-adhesion properties to both bacteria and new granulation tissue, which is conducive to exerting the positive effect of exudate on wound healing and preventing tissue avulsion when replacing dressings. In vivo excisional wound healing study and histological analysis confirmed the favorable effects of the loaded MSC-SLP in dressings on wound repair. The synergetic effects of the multifunctions of SWD and the efficient paracrine effect of MSC-SLP enable the wound healing rate be improved by up to 30%. Pathological and serum biochemical analysis indicated that the application of PDMS and poloxamer hydrogels loaded with MSC-SLP had little side effect on the blood biochemical indicators and the functions and metabolism of main organs of mice, demonstrating good biocompatibility, non-toxicity and bio-safety of the developed composite dressings. Compared to existing dressings, the developed novel multi-functional composite dressings present advantages of eliminating adhesion between dressing and new granulation tissues, providing sustained pro-healing effect of MSC-SLP on wound repair, reducing bacteria induced wound infections and enhancing wound healing quality.

CRediT authorship contribution statement

Wu Duan: Conceptualization, Data curation, Formal analysis, Funding acquisition, Investigation, Methodology, Validation, Writing – original draft. **Haipeng Wang:** Conceptualization, Data curation, Formal analysis, Funding acquisition, Investigation, Methodology,

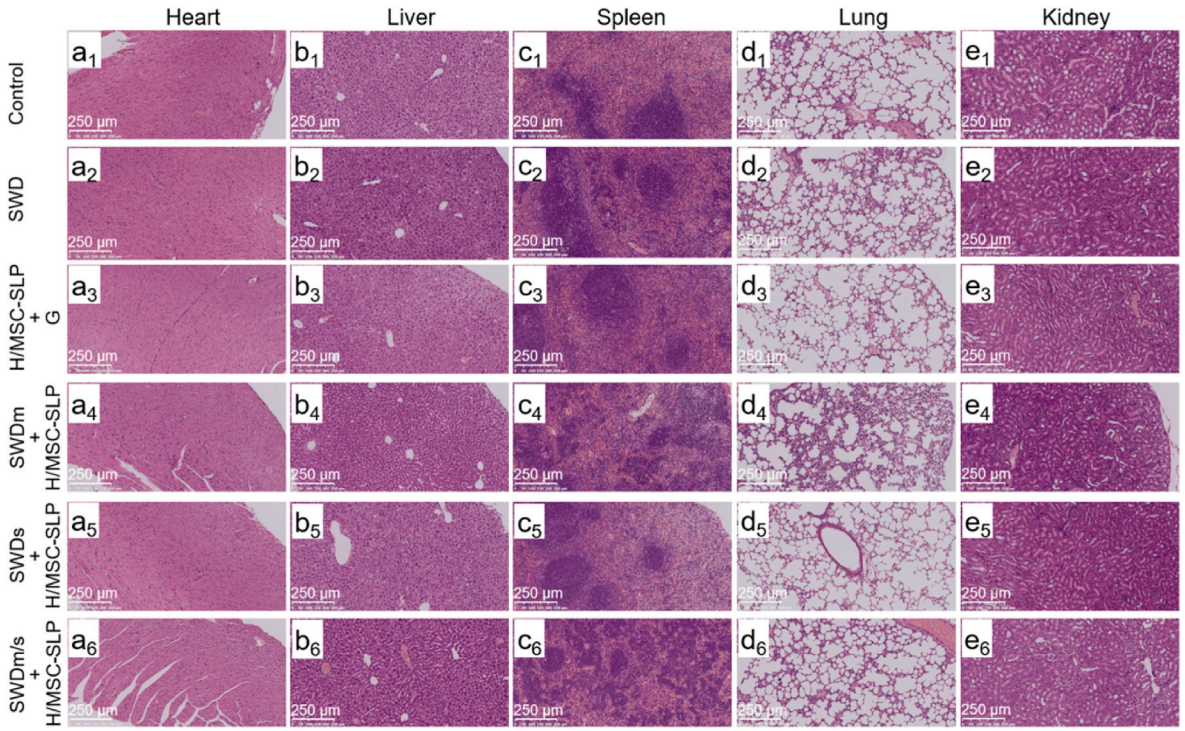

Fig. 7. H&E staining photos of heart, liver, spleen, lung, and kidney sections.

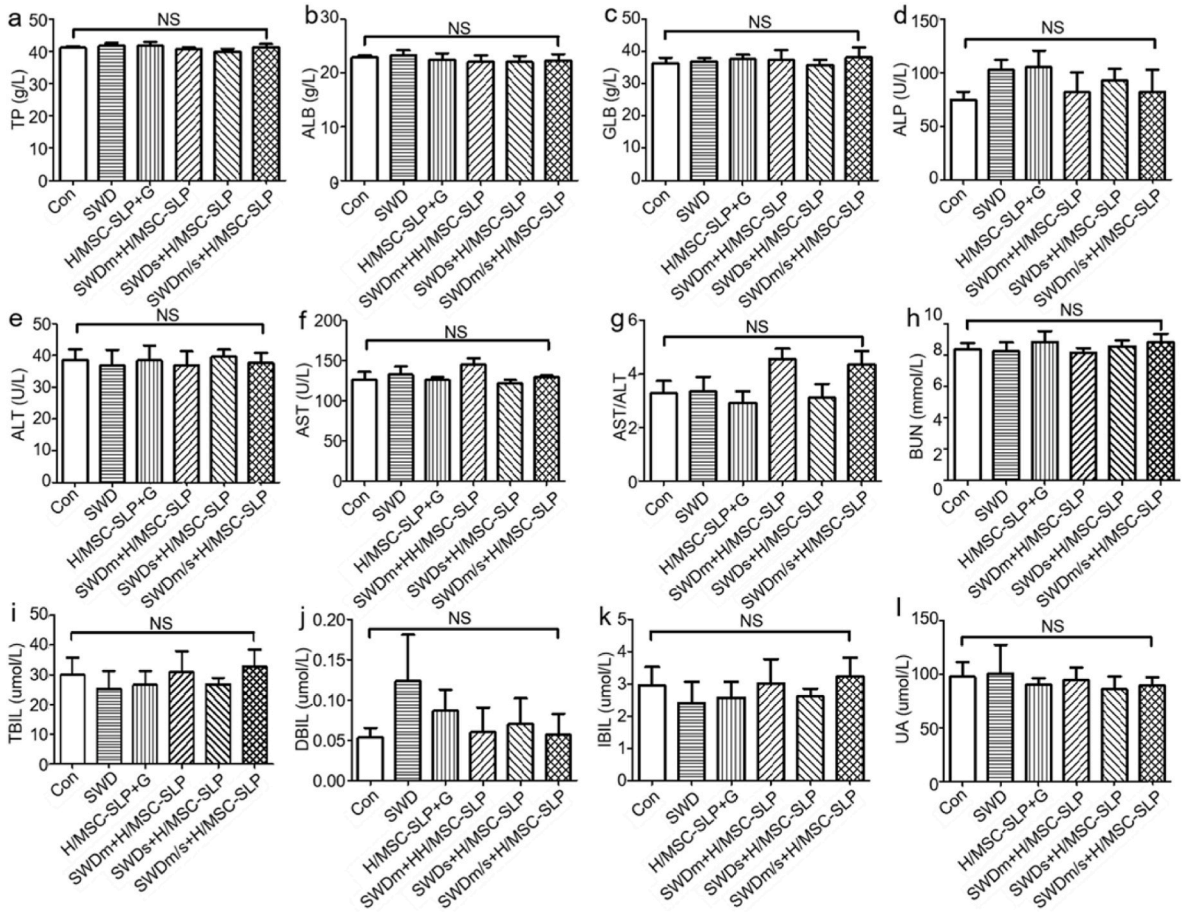

Fig. 8. Serum biochemical test results of mice in different treatment groups. Serum indexes including (a) total protein (TP), (b) albumin (ALB), (c) globulin (GLB), (d) alkaline phosphatase (ALP), (e) alanine transaminase (ALT), (f) aspartate transaminase (AST), (g) AST/ALT, (h) blood urea nitrogen (BUN), (i) total bilirubin (TBIL), (j) direct bilirubin (DBIL), (k) indirect bilirubin (IBIL), and (l) uric acid (UA).

Validation, Writing – original draft. **Ziran Wang:** Formal analysis. **Zhongjing Ren:** Methodology. **Xinxin Li:** Methodology. **Falian He:** Resources. **Shaomin Li:** Formal analysis, Methodology. **Yingchun Guan:** Investigation. **Fuqiang Liu:** Data curation. **Li Chen:** Project administration, Supervision. **Peng Yan:** Investigation, Supervision, Writing – review & editing. **Xinguo Hou:** Supervision.

Declaration of competing interest

The authors declare that they have no known competing financial interests or personal relationships that could have appeared to influence the work reported in this paper.

Data availability

Data will be made available on request.

Acknowledgements

This work was supported by the Shandong Provincial Natural Science Foundations (ZR2020QH085 and ZR2021QE077), Shandong Provincial Postdoctoral Innovation Project (202101004), the Endocrine and Metabolic Talent Research Project supported by China International Medical Foundation (2021-N-03), China Postdoctoral Science Foundation funded project (2022M721957), and the Taishan Industry Leading Talent Project of Shandong Province.

Appendix B. Supplementary data

Supplementary data to this article can be found online at https://doi.org/10.1016/j.mtbio.2024.100979.

References

[1] S. Thomas, Assessment and management of wound exudate, J. Wound Care 6 (7) (1997) 327–330.
[2] L. Mao, S. Hu, Y. Gao, L. Wang, W. Zhao, L. Fu, H. Cheng, L. Xia, S. Xie, W. Ye, Z. Shi, G. Yang, Biodegradable and Electroactive regenerated bacterial cellulose/MXene ($Ti_3C_2T_x$) composite hydrogel as wound dressing for accelerating skin wound healing under electrical stimulation, Adv. Healthcare Mater. 9 (2020) 2000872.
[3] M. Romanelli, K. Vowden, D. Weir, Exudate Management Made Easy, Wounds Int., 2010, pp. 1–6.
[4] W. Liu, C. Yang, R. Gao, C. Zhang, W. Ou-Yang, Z. Feng, C. Zhang, X. Pan, P. Huang, D. Kong, W. Wang, Polymer composite sponges with inherent antibacterial, hemostatic, inflammation-modulating and proregenerative performances for methicillin-resistant Staphylococcus aureus-infected wound healing, Adv. Healthcare Mater. 10 (2021) 2101247.
[5] N. Lohmann, L. Schirmer, P. Atallah, E. Wandel, R.A. Ferrer, C. Werner, J.C. Simon, S. Franz, U. Freudenberg, Glycosaminoglycan-based hydrogels capture inflammatory chemokines and rescue defective wound healing in mice, Sci. Transl. Med. 9 (2017) eaai9044.
[6] Y.S. Zhang, A. Khademhosseini, Advances in engineering hydrogels, Science 356 (2017) eaaf3627.
[7] J. Xiang, R. Zhu, S. Lang, H. Yan, G. Liu, B. Peng, Mussel-inspired immobilization of zwitterionic silver nanoparticles toward antibacterial cotton gauze for promoting wound healing, Chem. Eng. J. 409 (2021) 128291.
[8] W. Zheng, C. Chen, X. Zhang, X. Wen, Y. Xiao, L. Li, X. Liu, Layer-by-layer coating of carboxymethyl chitosan-gelatin-alginate on cotton gauze for hemostasis and wound healing, Surf. Coating. Technol. 406 (2021) 126644.
[9] B. Lu, X. Han, D. Zou, X. Luo, L. Liu, J. Wang, M.F. Maitz, P. Yang, N. Huang, A. Zhao, Catechol-chitosan/polyacrylamide hydrogel wound dressing for regulating local inflammation, Mater, Today Bio 16 (2022) 100392.
[10] H. Liu, X. Zhu, H. Guo, H. Huang, S. Huang, S. Huang, W. Xue, P. Zhu, R. Guo, Nitric oxide released injectable hydrogel combined with synergistic photothermal therapy for antibacterial and accelerated wound healing, Appl. Mater. Today 20 (2020) 100781.
[11] K. Skórkowska-Telichowska, M. Czemplik, A. Kulma, J. Szopa, The local treatment and available dressings designed for chronic wounds, J. Am. Acad. Dermatol. 68 (2013) e117–e126.
[12] Y. Wang, Y. Jin, W. Chen, J. Wang, H. Chen, L. Sun, X. Li, J. Ji, Q. Yu, L. Shen, B. Wang, Construction of nanomaterials with targeting phototherapy properties to inhibit resistant bacteria and biofilm infections, Chem. Eng. J. 358 (2019) 74–90.
[13] S. Zhang, J. Hou, Q. Yuan, P. Xin, H. Cheng, Z. Gu, J. Wu, Arginine derivatives assist dopamine-hyaluronic acid hybrid hydrogels to have enhanced antioxidant activity for wound healing, Chem. Eng. J. 392 (2020) 123775.
[14] H. Li, J. Yang, Z. Xu, Asymmetric surface engineering for Janus membranes, Adv. Mater. Interfac. 7 (2020) 1902064.
[15] L. Shi, X. Liu, W. Wang, L. Jiang, S. Wang, A self-pumping dressing for draining excessive biofluid around wounds, Adv. Mater. 31 (2019) 1804187.
[16] Z. Luo, L. Jiang, C. Xu, D. Kai, X. Fan, M. You, C.M. Hui, C. Wu, Y.-L. Wu, Z. Li, Engineered Janus amphipathic polymeric fiber films with unidirectional drainage and anti-adhesion abilities to accelerate wound healing, Chem. Eng. J. 421 (2021) 127725.
[17] H. Zhang, C. Chen, H. Zhang, G. Chen, Y. Wang, Y. Zhao, Janus medical sponge dressings with anisotropic wettability for wound healing, Appl. Mater. Today 23 (2021) 101068.
[18] Q. Zhang, Y. Li, Y. Yan, X. Zhang, D. Tian, L. Jiang, Highly flexible monolayered porous membrane with superhydrophilicity-hydrophilicity for unidirectional liquid penetration, ACS Nano 14 (2020) 7287–7296.
[19] W. Li, Q. Yu, H. Yao, Y. Zhu, Paul D. Topham, K. Yue, L. Ren, L. Wang, Superhydrophobic hierarchical fiber/bead composite membranes for efficient treatment of burns, Acta Biomater. 92 (2019) 60–70.
[20] X. Zhang, R. Lv, L. Chen, R. Sun, Y. Zhang, R. Sheng, T. Du, Y. Li, Y. Qi, A multifunctional Janus electrospun nanofiber dressing with biofluid draining, monitoring, and antibacterial properties for wound healing, ACS Appl. Mater. Interfaces 14 (2022) 12984–13000.
[21] B. Xu, A. Li, R. Wang, J. Zhang, Y. Ding, D. Pan, Z. Shen, Elastic Janus film for wound dressings: unidirectional biofluid transport and effectively promoting wound healing, Adv. Funct. Mater. 31 (2021) 2105265.
[22] Z. Xu, C. Zhang, X. Wang, D. Liu, Release strategies of silver ions from materials for bacterial killing, ACS Appl. Bio Mater. 4 (2021) 3985–3999.
[23] H. Li, A. Granados, E. Fernández, R. Pleixats, A. Vallribera, Anti-inflammatory cotton fabrics and silica nanoparticles with potential topical medical applications, ACS Appl. Mater. Interfaces 12 (2020) 25658–25675.
[24] F. Wang, M. Sun, D. Li, X. Qin, Y. Liao, X. Liu, S. Jia, Y. Xie, C. Zhong, Multifunctional asymmetric bacterial cellulose membrane with enhanced anti-bacterial and anti-inflammatory activities for promoting infected wound healing, Small (2023) 2303591.
[25] L.Č. Ćurić, M. Šuligoj, M. Ibic, N. Marovič, B. Vihar, M. Vesenjak, P.D. Dubrovski, N. Novak, J. Stergar, I. Ban, U. Maver, M. Milojević, T. Maver, Development of a novel NiCu nanoparticle-loaded polysaccharide-based hydrogel for 3D printing of customizable dressings with promising cytotoxicity against melanoma cells, Mater, Today Bio 22 (2023) 100770.
[26] T. Li, Q. Bao, J. Shen, R.V. Lalla, D.J. Burgess, Mucoadhesive in situ forming gel for oral mucositis pain control, Int. J. Pharm. (Amst.) 580 (2020) 119238.
[27] Z. Han, L. Dong, A. Li, Z. Li, L. Fu, Z. Zhang, X. Li, X. Li, Efficient angiogenesis-based wound healing through hydrogel dressing with extracellular vesicles release, Mater. Today Bio 16 (2022) 100427.
[28] L. Du, X. Feng, X. Xiang, Y. Jin, Wound healing effect of an in situ forming hydrogel loading curcumin-phospholipid complex, Curr. Drug Deliv. 13 (2016) 76–82.
[29] S. Wang, Y. Zhang, F. Sun, K. Xi, Z. Sun, X. Zheng, F. Guo, H. Zhong, M. Yang, Y. Shao, B. Huang, M. Dong, S. Ni, L. Sun, Catalase-like nanozymes combined with hydrogel to facilitate wound healing by improving the microenvironment of diabetic ulcers, Mater. Des. 225 (2023) 111557.
[30] D. Liu, T. Jiang, W. Cai, J. Chen, H. Zhang, S. Hietala, H.A. Santos, G. Yin, J. Fan, An in situ gelling drug delivery system for improved recovery after spinal cord injury, Adv. Healthcare Mater. 5 (2016) 1513–1521.
[31] H. Wang, W. Duan, Z. Ren, X. Li, W. Ma, Y. Guan, F. Liu, L. Chen, P. Yan, X. Hou, Engineered sandwich-structured composite wound dressings with unidirectional drainage and anti-adhesion supporting accelerated wound healing, Adv. Healthcare Mater. 12 (2023) 2202685.
[32] H. Wang, Q. Zhang, X. Li, P. Yan, Y. Guan, High precision dynamic manipulations of large-volume-range water-based droplets by a soft gripper with robust water-repellent superhydrophobic surface, Adv. Mater. Technol. 8 (2023) 2201599.
[33] Z. Luo, L. Jiang, C. Xu, D. Kai, X. Fan, M. You, C.M. Hui, C. Wu, Y.-L. Wu, Z. Li, Engineered Janus amphipathic polymeric fiber films with unidirectional drainage and anti-adhesion abilities to accelerate wound healing, Chem. Eng. J. 421 (2021) 127725.
[34] H. Wang, M. He, H. Liu, Y. Guan, One-step fabrication of robust superhydrophobic steel surfaces with mechanical durability, thermal stability, and anti-icing function, ACS Appl. Mater. Interfaces 11 (2019) 25586–25594.
[35] H. Wang, M. He, H. Liu, Y. Guan, Controllable water behaviors on V-shape micro-grooved titanium alloy surfaces depending on the depth-to-width aspect ratio, Mater. Today Phys. 20 (2021) 100461.
[36] E. Zhao, H. Liu, Y. Jia, T. Xiao, J. Li, G. Zhou, J. Wang, X. Zhou, X.-J. Liang, J. Zhang, Z. Li, Engineering a photosynthetic bacteria-incorporated hydrogel for infected wound healing, Acta Biomater. 141 (2022) 302–313.
[37] R. Huang, M. Hu, W. Liang, J. Zheng, Y. Du, Y. Lin, H. Wang, W. Guo, Z. Zeng, C. Li, M. Li, H. Wang, X. Zhang, One-step preparation of green fabric for continuous antibacterial applications, Engineering 7 (2021) 326–333.
[38] S. Naderizadeh, S. Dante, P. Picone, M.D. Carlo, R. Carzino, A. Athanassiou, I. S. Bayer, Bioresin-based superhydrophobic coatings with reduced bacterial adhesion, J. Colloid Interface Sci. 574 (2020) 20–32.
[39] Z. Montgomerie, K.C. Popat, Improved hemocompatibility and reduced bacterial adhesion on superhydrophobic titania nanoflower surfaces, Mater. Sci. Eng. C 119 (2021) 111503.
[40] E.J. Falde, S.T. Yohe, Y.L. Colson, M.W. Grinstaff, Superhydrophobic materials for biomedical applications, Biomaterials 104 (2016) 87–103.
[41] A.C. Lima, J.F. Mano, Micro/nano-structured superhydrophobic surfaces in the biomedical field: part II: applications overview, Nanomedicine 10 (2015) 271–297.

[42] X. An, W. Li, Y. Zhang, J. Ding, S. Zhang, T. Hu, S. Li, Y. Ren, P. Liu, X. Li, Antibacterial and superhydrophobic hemostatic properties of fluorinated random copolymer composite nanocoatings, Prog. Org. Coating 168 (2022) 106869.
[43] S. Chen, S. Li, Z. Ye, Y. Zhang, S. Gao, H. Rong, J. Zhang, L. Deng, A. Dong, Superhydrophobic and superhydrophilic polyurethane sponge for wound healing, Chem. Eng. J. 446 (2022) 136985.
[44] H. Liu, Z. Liang, F. Wang, C. Zhou, X. Zheng, T. Hu, X. He, X. Wu, P. Lan, Exosomes from mesenchymal stromal cells reduce murine colonic inflammation via a macrophage-dependent mechanism, JCI Insight 4 (2019) e131273.
[45] J. Obendorf, C. Fabian, U.H. Thome, M. Laube, Paracrine stimulation of perinatal lung functional and structural maturation by mesenchymal stem cells, Stem Cell Res. Ther. 11 (2020) 525.
[46] N.V. Bogatcheva, M.E. Coleman, Conditioned medium of mesenchymal stromal cells: a new class of therapeutics, Biochemistry (Mosc.) 84 (2019) 1375–1389.
[47] X. He, Z. Dong, Y. Cao, H. Wang, S. Liu, L. Liao, Y. Jin, L. Yuan, B. Li, MSC-derived exosome promotes M2 polarization and enhances cutaneous wound healing, Stem Cell. Int. (2019) 7132708.
[48] S. Zhang, K.Y.W. Teo, S.J. Chuah, R.C. Lai, S.K. Lim, W.S. Toh, MSC Exosomes Alleviate Temporomandibular Joint Osteoarthritis by Attenuating Inflammation and Restoring Matrix Homeostasis, vol. 200, 2019, pp. 35–47.
[49] B. Chen, Y. Sun, J. Zhang, Q. Zhu, Y. Yang, X. Niu, Z. Deng, Q. Li, Y. Wang, Human embryonic stem cell-derived exosomes promote pressure ulcer healing in aged mice by rejuvenating senescent endothelial cells, Stem Cell Res. Ther. 10 (2019) 142.
[50] Y. Luo, L. Xie, A. Mohsin, W. Ahmed, C. Xu, Y. Peng, H. Hang, Y. Zhuang, J. Chu, M. Guo, Efficient generation of male germ-like cells derived during co-culturing of adipose-derived mesenchymal stem cells with Sertoli cells under retinoic acid and testosterone induction, Stem Cell Res. Ther. 10 (2019) 358.
[51] S. Tao, S. Guo, M. Li, Q. Ke, Y. Guo, C. Zhang, Chitosan wound dressings incorporating exosomes derived from MicroRNA-126-overexpressing synovium mesenchymal stem cells provide sustained release of exosomes and heal full-thickness skin defects in a diabetic rat model, Stem Cells Transl. Med. 6 (2017) 736–747.
[52] R. Tutuianu, A. Rosca, D.M. Iacomi, M. Simionescu, I. Titorencu, Human mesenchymal stromal cell-derived exosomes promote in vitro wound healing by modulating the biological properties of skin keratinocytes and fibroblasts and stimulating angiogenesis, Int. J. Mol. Sci. 22 (2021) 6239.
[53] S. Wang, Y. Zhang, F. Sun, K. Xi, Z. Sun, X. Zheng, F. Guo, H. Zhong, M. Yang, Y. Shao, B. Huang, M. Dong, S. Ni, L. Sun, Catalase-like nanozymes combined with hydrogel to facilitate wound healing by improving the icroenvironment of diabetic ulcers, Mater. Des. 225 (2023) 111557.
[54] H.E. Albott, S. Mascharak, M. Griffin, D.C. Wan, M.T. Longaker, Wound healing, fibroblast heterogeneity, and fibrosis, Cell Stem Cell 29 (2022) 1161–1180.
[55] N.B. Vu, H.T. Nguyen, R. Palumbo, R. Pellicano, S. Fagoonee, P.V. Pham, Stem cell-derived exosomes for wound healing: current status and promising directions, Minerva Med. 112 (2021) 384–400.